On the observed and modeled development of Hurricane Earl (2010) during rapid intensification

JOSHUA ALLAND AND TSING-CHANG CHEN

Department of Geological and Atmospheric Sciences, Iowa State University, Ames, IA

SUNDARARAMAN GOPALAKRISHNAN, THIAGO QUIRINO, HUA CHEN, AND XUEJIN ZHANG

NOAA/Hurricane Research Division/Atlantic Oceanographic Meteorological Laboratory, Miami, FL

ABSTRACT

Forecasting tropical cyclone (TC) intensification remains difficult despite research efforts to improve numerical weather prediction models. This study aims to examine Hurricane Earl's rapid intensification in order to gain a better understanding of the observed and modeled intensification process. 113 dropwindsondes were analyzed before, during, and after RI in the eye, eyewall, and outer rainband to study the evolution of the thermodynamic and dynamic vertical profiles at these locations. Afterword, modeled vertical thermodynamic and wind profiles were analyzed with the dropwindsonde data to determine how the Hurricane Forecast Research and Forecasting (HWRF) System modeled the rapid intensification of Hurricane Earl. Thereafter, idealized warm core structures were analyzed to develop a theory as to how the structure of the warm core affects the minimum sea level pressure (MSLP). This theory was compared to Hurricane Earl's warm core. Results show the development of a subsidence-induced dry layer in the eye and a saturated column in the eyewall. Additionally, neither the difference in the observed and modeled temperature, wind speed, or wind direction statistically influenced the difference in the observed and modeled MSLP. Furthermore, the depth of the warm core was determined as the most important factor in altering the MSLP of a TC, with the large depth of Hurricane Earl's warm core contributing to its RI.

1. Introduction

Although tropical cyclone (TC) track forecasting has improved within the last 10 years, intensification forecasting remains difficult (Houze et al. 2006). Rapid intensification (RI), defined as at least a 42 hPa day^{-1} drop in minimum central pressure (Holliday and Thompson 1979) or at least a 15.4 m s^{-1} day^{-1} increase in the maximum surface wind (Kaplan and DeMaria 2003), is especially difficult to forecast. TCs have the potential to cause severe destruction to property and widespread loss of life, so it is important to improve operational numerical weather prediction (NWP) models to mitigate these effects.

Certain environmental conditions are known to enhance intensification of TCs, namely warm sea surface temperatures (SSTs), moist mid-level air advected into the inner core, and vertical wind shear of less than 15 knots from 850 hPa to 200 hPa (e.g., Gopalakrishnan et al. 2010). Other smaller-scale features also influence intensification including convective asymmetries around the vortex, wind gusts, aerosols, and microphysical processes, such as evaporation (e.g., Gopalakrishnan et al. 2010). Forecasting TC intensification remains difficult because these small-scale features are not well resolved by the current model resolutions. Parameterizations are necessary to represent these small-scale features, which are not always accurate (Gopalakrishnan et al. 2011).

The intensification problem has resulted in the formation of the Hurricane Forecast Improvement Project (HFIP). Formed by the National Oceanic

and Atmospheric Administration (NOAA), HFIP aims to double the accuracy of tropical cyclone intensity forecasts in 10 years (e.g., Gopalakrishnan et al. 2011). To improve intensification forecasting, researchers at the Hurricane Research Division (HRD), among other places, aim to improve NWP models by increasing the horizontal resolution and by examining the accuracy of parameterization schemes. The goal is to accurately simulate the development, intensification, maintenance, and eventual dissipation of TCs.

2. Properties of a TC

It is vital to understand the general structure of a TC in order to accurately simulate TC intensification. The inner core of a TC generally consists of a central low-pressure system with winds traveling counterclockwise around the low (in the northern hemisphere). Above the planetary boundary layer (PBL), these winds are approximately in gradient wind balance, meaning that the pressure gradient force (PGF) balances the Coriolis and centrifugal forces. This tangential circulation is called the primary circulation (e.g., Holton 2004). Near the surface, friction turns the horizontal winds inward toward the low. This inflow layer advects moist enthalpy into the storm from the sea surface (e.g., Willoughby 1998).

The outer eye has near-surface horizontal winds with a component traveling radially outward due to supergradient winds in this region (e.g., Smith 1980). Strong convergence occurs where these winds collide with the inflow layer, a region known as the eyewall. The strong convergence produces deep convection and latent heat release from condensation, with vertically moving air diverging in the upper atmosphere to form the outflow region. The combination of the inflow layer near the surface, upward motion in the eyewall, and eventual divergence aloft is known as the secondary circulation (e.g., Holton 2004).

As air is advected away from the eye, mass conservation requires subsidence in the eye (e.g., Willoughby 1998). The subsiding air originates from the outflow layer aloft and detrainment of air from the eyewall. Zhang and Chen proposed that the subsiding air has its origins in the stratosphere (2012), but this is solely speculation. Smith discussed the importance of subsidence, as it maintains hydrostatic balance between the perturbation pressure and buoyancy force (1980).

Subsidence in the eye is important in maintaining the strength of a TC. The combination of subsidence in the eye and detrainment of heat from the eyewall produces a warm core in the mid- to upper- troposphere (e.g., Willoughby 1998). This warming results in a pressure drop at the surface, which strengthens the winds near the surface and hence, strengthens the TC itself.

The development of the warm core is a topic of discussion in recent literature. For example, does the warm core develop from a symmetric inflow layer that produces widespread vertical motion or does the warm core develop from individual, asymmetric vertical motions? Current theories suggest that intensification results from individual, asymmetric plumes of vertical motion, which release heat from condensation and amplify the warm core (Nguyen et al. 2008; Montgomery et al. 2009; Smith et al. 2008, 2009). Convective bursts, which are intense updrafts in mesoscale convective systems (MCSs), have been considered to be large contributors to RI. Observational studies show that convective bursts either preceded or occurred simultaneously with the onset of RI (Zhang and Chen 2012).

Gopalakrishnan et al. proposed that intensification is the result of asymmetric thermal plumes. They found that these plumes, which have tangentially averaged vertical velocities of only 3-5 m s^{-1}, carry the bulk of the heat and moisture from the boundary layer into a TC (2010). The rapid development of a modeled warm core was found to coincide with the onset of these moist thermal plumes.

It is known that the outflow layer influences the maintenance of the warm core. Since the warm core and outflow layer generally coexist between 13-15 km, the ventilation from the outflow layer protects the warm core from environmental flows (Zhang and Chen 2012). It is important to understand the development and maintenance of the warm core because the warm core is essential to TC intensification. Since hydrostatic balance holds within a TC (Haurwitz 1935), a derived version of the hydrostatic approximation is represented by

$$P_1 = P_2 e^{\frac{(z_2 - z_1)g}{R_d T}}, \qquad (1)$$

where P_1 is the pressure at a lower height z_1, P_2 is the pressure at a higher height z_2, g is the standard gravity, R_d is the gas constant for dry air, and T is the layer-mean temperature in the layer from z_1 to z_2. From this equation, it is evident that the minimum sea level pressure (MSLP) will decrease with an increase in the layer mean temperature. Thus, the warming associated with a warm core lowers the MSLP and strengthens a TC.

3. Data methods and procedures

a. Objectives

This study aims to examine the observed and modeled rapid intensification of Hurricane Earl. First, observational data is analyzed to determine how the thermodynamic and dynamic structure of Earl changes with time. Afterword, model data using the Hurricane Research and Forecasting (HWRF) System is compared to the observational data to determine the accuracy of the model forecast. Differences in the observed and modeled thermodynamic and dynamic structures at the mandatory levels in the atmosphere (850 hPa, 700 hPa, 500 hPa, and 200 hPa) are compared to the observed and modeled MSLP to determine if these thermodynamic and dynamic differences contribute to a significant difference in the observed and modeled MSLP. This will give insight into the causes of inaccurate MSLP estimates by the HWRF model and ultimately, will give insight into better intensification forecasting.

Thereafter, this study aims to understand the development of a warm core in the eye of a TC. For example, does the height and depth of a warm core produce a significant change in the corresponding MSLP? Idealized warm cores are studied to suggest the importance of the height and depth of the warm core. This theory is later compared to the development of Hurricane Earl's warm core.

Hurricane Earl is studied due to the unprecedented observational and model dataset, as there were 113 dropwindsondes released, continuous radar coverage during the mission flights, and 1-minute model output. Additionally, Hurricane Earl remained distant from land, which simplified the analysis of Earl's thermodynamic and dynamic processes. This study is part of a larger project by HRD to examine the modeled intensification of Hurricane Earl.

A better understanding of the modeled intensification process using a next-generation TC model, the HWRF model, is vital in order to improve NWP models. More accurate NWP models will better predict TC intensification, which will save property and lives. Additionally, more accurate forecasts will allow rescue teams to more confidently prepare for major landfalls of TCs.

b. Observed dropwindsonde dataset

113 dropwindsondes were analyzed between 0000 UTC on 28 August and 0000 UTC on 1 September. RI began on 29 August at 0600 UTC and ended on 30 August at 0600 UTC, so the dropwindsonde data included the RI period. The vertical profiles of temperature, relative humidity, zonal wind, meridional wind, and geopotential height were recorded by every dropwindsonde. Some levels had missing values for temperature or relative humidity so linear interpolation was completed using points above and below the missing value. This was done so ample points were recorded on the temperature soundings.

The dropwindsonde data did not give the dewpoint temperature but instead, recorded the relative humidity. Because of this, the dewpoint temperature was calculated from the known values of relative humidity and temperature. The Clausius-Clapeyron equation, given by equation (2)

$$e_s = 10^{9.4041 - \frac{2.354 \times 10^3}{T + 273.15}}, \qquad (2)$$

was used to calculate the saturation vapor pressure, where e_s is the saturation vapor pressure (hPa) and T is the temperature (°C) at a given level. Then, the vapor pressure was determined from the relation between relative humidity and saturation vapor pressure using equation (3)

$$e = \frac{RH}{100} \times e_s, \qquad (3)$$

where RH is the relative humidity at a given level. Afterword, the dewpoint temperature at a specific level was calculated using the Clausius-Clapeyron equation again, but with using the vapor pressure as the input variable. This is given by equation (4)

$$T_d = \frac{2.354 \times 10^3}{-\log_{10}(e) + 9.4041} - 273.15, \qquad (4)$$

where T_d is the dewpoint temperature (K). Additionally, the geopotential height was only given for the mandatory levels in the atmosphere. The geopotential height for the non-mandatory levels was estimated using a simplified version of the thickness equation

$$z = -\frac{R_d \times \frac{(T + 273.15) + (T_o + 273.15)}{2}}{g} \times \ln(\frac{P}{P_o}) + z_o, \qquad (5)$$

where T and P are the temperature and pressure at a given level, T_o and P_o are the temperature and pressure at the final recorded level in the dropwindsonde data (closest level to the surface), z_o is the geopotential height at the final recorded level, and R_d is gas constant for dry air. Note that this equation assumes an average temperature from the surface to the height of interest.

Vertical thermodynamic profiles were created for each dropwindsonde to determine how the thermodynamic structure of Hurricane Earl evolved with time. These soundings were plotted using a NCAR Command Language (NCL) script. Afterword, these profiles were separated into three temporal groups: pre-RI, RI, and post-RI. These three groups were further separated into three spatial groups, the eye, eyewall, and the outer rainband, depending on their release location within the TC. The goal was to analyze how the vertical thermodynamic profile evolved with time for each of the three locations. It was hypothesized that the eye region would develop a well-defined mid- and upper-level dry layer due to subsidence within the upper troposphere of the eye. It was also hypothesized that the temperature would increase in the mid- and upper- levels of the eye due to the development of a defined warm core. Further, it was expected that the eyewall region would become saturated at the surface with an increasing saturation depth with time due to the development of deep cumulus convection. The outer rainband region was expected to be unsaturated throughout the forecast period, as this region generally consists of both stratiform precipitation and dry slots due to downward motion. The analysis of the dropwindsondes at different times and locations will be useful in analyzing how Hurricane Earl developed and rapidly intensified. For example, did the dry layer and warming in the eye rapidly develop when RI began? Additionally, this analysis will give insight into how the vertical thermodynamic and dynamic structures of a TC evolves within the eye, eyewall, and outer rainband before, during, and after RI. This will be useful to forecasters at the National Hurricane Center (NHC), who can use vertical profiles from dropwindsonde data in the eye, eyewall, and outer rainband to predict whether a TC will likely intensify.

c. Modeled dataset

1) THE HWRF MODEL

Version 3.2 of the HWRF model is formulated on a rotated latitude-longitude Arakawa E-grid with a pressure-sigma hybrid coordinate in the vertical (Gopalakrishnan et al. 2010). There are three domains: a stagnant parent domain at 27 km horizontal resolution, a low resolution inner domain at 9 km, and a high resolution inner domain at 3 km (Gopalakrishnan, personal communication). The moving nest provides high resolution coverage in the inner core of the TC. This is essential to improve intensity forecasts, as the higher resolution will be able to better depict atmospheric processes important to intensification. The moving nest can travel anywhere within the grid points of the integration domain (Gopalakrishnan et al. 2010), with the center of the moving nest being the lowest pressure within the nest domain (Gopalakrishnan et al. 2006).

The model is initialized with the operational Geophysical Fluid Dynamics Laboratory (GFDL) model conditions, with the outer domain's lateral boundary conditions updated with the Global Forecast System (GFS) data every three hours (Gopalakrishnan et al. 2011). The model vortex is initialized from the GFS, with subsequent cycles adjusting to the intensity estimated by the NHC. All meteorological fields (except mass and moisture) are bi-linearly interpolated along the horizontal direction from the parent grid onto the nested domain (Gopalakrishnan et al. 2006). The model forecast calculates the meteorological variables in small time steps and integrates these values to predict the evolution of the atmosphere and the storm itself (Gopalakrishnan et al. 2011).

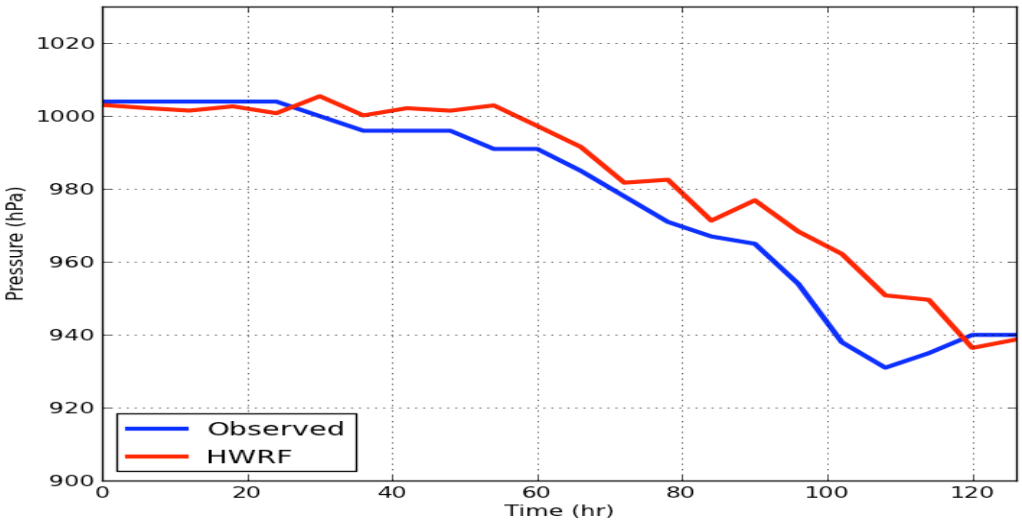

FIG. 1. HWRF 126-hour MSLPforecast (red) and observations (blue) at 1800 UTC on 26 August 2010.

(a)

(b)

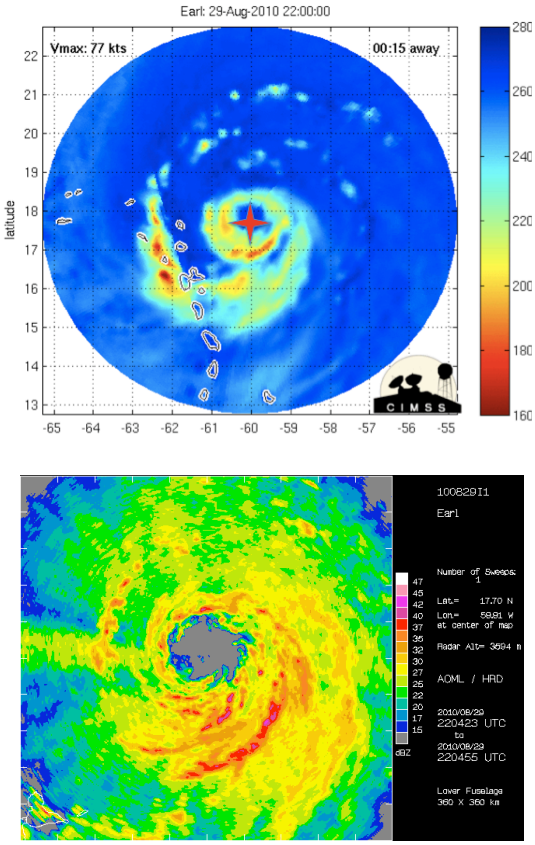

FIG. 2. (a) Morphed integrated microwave imagery and (b) corresponding radar reflectivity while flying in the eye of Hurricane Earl at 2203 UTC on 29 August 2010.

HRD's diagnostic postprocessor, Diapost, reads the model's output and transforms the variables from the model grid to a grid useful for doing TC diagnostics, such as a latitude-longitude grid or a storm-centered cylindrical grid (Gopalakrishnan et al. 2011).

2) COMPARISON OF MODEL OUTPUT TO OBSERVATIONS

Fig. 1 shows the modeled intensification of Hurricane Earl, beginning on 26 August at 1800 UTC and ending on 1 September at 0000 UTC, thus running for 126 hours. This forecast time was chosen to compare with the observational dataset because the HWRF model accurately forecasted the development and RI of Hurricane Earl. This is important, as the accurate model forecast is directly compared to observations to determine if the model accurately simulated the thermodynamic and dynamic structure of Hurricane Earl, and whether discrepancies between observed and modeled variables inaccurately altered the predicted MSLP of the model. This comparison may give insight into the modeled intensification process of TCs in the HWRF model.

Model observations for temperature, dewpoint, wind speed, and wind direction were available every minute at 3-km horizontal resolution. First, the modeled vertical thermodynamic structure was compared to the dropwindsonde profiles at the dropwindsonde release locations. Morphed integrated microwave imagery and in-flight radar data (Figs. 2a and 2b) were used to determine the

exact location of the dropwindsonde release point within Hurricane Earl. Once this was determined, a generated Grid Analysis and Display System (GrADS) script was used to determine the vertical thermodynamic structure in the model. The GrADS script was used by clicking on a point in the modeled TC that corresponded to the same location as the dropwindsonde release point. Then, the modeled vertical thermodynamic profile was compared to the dropwindsonde observations. A temperature difference between the dropwindsonde and model temperatures values was computed at every mandatory level using equation (6)

$$T_{DIFF} = T_{OB} - T_M, \qquad (6)$$

where T_{OB} and T_M are the observed and modeled temperatures at a given level, respectively. This difference was compared to the difference between the modeled and observed MSLP of Hurricane Earl at the same times and locations as the dropwindsonde release points. Statistical analysis was completed to determine if there was a statistically significant linear relationship between the temperature difference and difference in MSLP. It was hypothesized that a temperature difference would correspond to a statistically significant difference in the MSLP, as warming (cooling) in the eye, eyewall, or outer-rainband would theoretically produce a lower (higher) MSLP once the relatively warm (cool) air is advected to the center of the TC.

It is also important to compare the wind speed and direction of the HWRF model to observations. The wind affects the movement of moist enthalpy within a TC, so an accurate simulation of the wind is vital in order to have a robust model forecast. The modeled wind speed and direction were compared to the observed dropwindsonde data at the mandatory levels. The dropwindsonde data gave the zonal and meridional wind speed, so the total wind speed and direction was calculated from these values.

It was hypothesized that a larger difference in the wind speed and direction would result in a greater deviation of the modeled MSLP compared to observations. This prediction was made simply because a greater deviation in the wind would cause enthalpy-rich air to travel to a different location at a different speed in Hurricane Earl, affecting the location of warming within the eye of the TC. It was also hypothesized that deviations in the wind speed and direction in the mid-levels (850 hPa and 700 hPa) would cause greater deviations in the modeled MSLP compared to observations because warm, enthalpy-rich air is generally located at these levels. Note that for every difference, the modeled value is subtracted from the observed value.

d. Analysis of Earl's warm core

It is important to understand where the warm core develops because this will affect the resulting drop in MSLP. According to Zhang and Chen, higher-level warming can produce a much greater pressure fall at the surface due to the exponential effects of upper-level warming. According to their understanding, a storm may cease to deepen after 22-24 hours if there is no upper-level warming (2012).

This study subsequently examines Zhang and Chen's assertion by evaluating idealized parabolic warm cores. A simple FORTRAN code was developed using (1) to determine the MSLP, given a specific warm core structure. In the code, (1) was integrated in vertical steps of 0.25 m to determine the pressure in each layer. The summation of these pressures from the top of the atmosphere to the surface resulted in the MSLP for a particular warm core structure. The vertical location and depth of the warm core were manipulated to determine how these factors affected the MSLP. It was hypothesized that a higher and deeper warm core would significantly lower the MSLP.

Once a general understanding of the influence of the warm core structure on the MSLP is determined, Hurricane Earl's warm core is studied using the HWRF model and vertical thermodynamic cross sections in GrADS to analyze how its warm core structure affected the MSLP, and if these results agree with the theory developed.

The objective is to determine how the HWRF model develops Hurricane Earl's warm core. For example, does the model develop its warm core in the upper or lower atmosphere? What was the resultant MSLP? Did this agree with theory? Answering these questions will allow forecasters to better understand how the warm core influences TC strength and intensification.

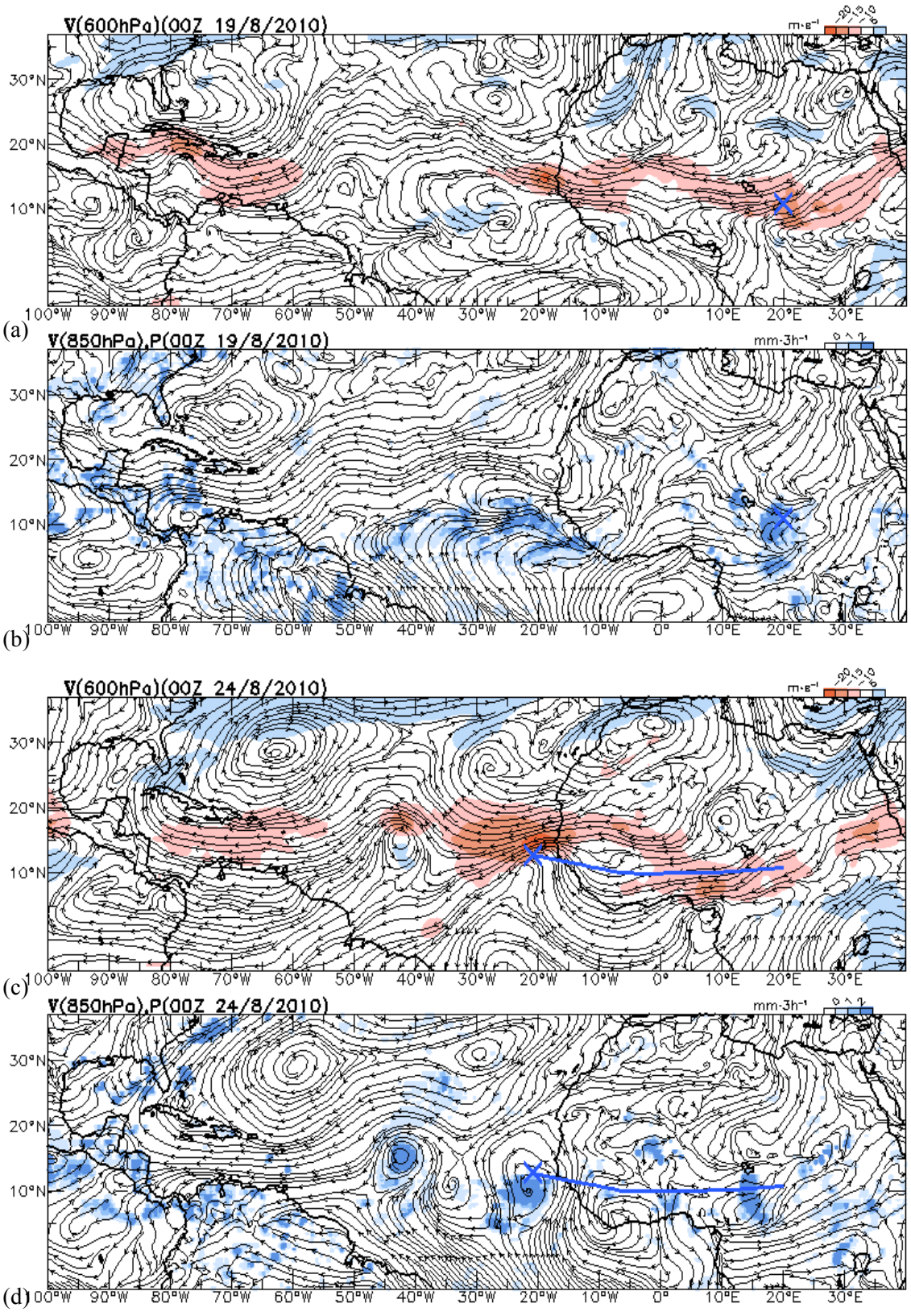

FIG. 3. (a) Streamlines (black) and the AFJ (orange) at 600 hPa during Hurricane Earl's genesis at 0000 UTC on 19 Aug. 2010, (b) Streamlines (black) and precipitation (blue) for the same time as a., (c) Streamlines (black) and the AFJ (orange) at 600 hPa after Hurricane Earl travels off the coast of western Africa at 0000 UTC on 24 Aug. 2010, (d) Streamlines (black) and precipitation (blue) at 850 hPa or the same time as (c).

4. Hurricane Earl's forecast

Hurricane Earl began as a strong tropical wave off the west coast of Africa on 23 August. By 25 August the wave developed into a tropical depression (Cangialosi 2010).

The operational models accurately forecasted Earl's track. The steering flow was well-established, with a subtropical high in the Atlantic that moved the storm westward. On 31 August the storm approached the southwest corner of the subtropical ridge, where it gradually turned west-northwest and later, northwest. By 2 September Earl moved northward along the zone of high pressure and by 4 September, it moved northeast as it was swept away by an upper-level trough.

The models also accurately forecasted the intensity forecast. On 27 August convection increased in the western semicircle of Earl, but northerly shear also increased. This shear, combined with dry air lurking near the cyclone, likely slowed intensification. By 28 August Earl intensified a bit due to warmer ocean waters, but northerly shear continued to increase. This northerly shear occurred from the outflow of Hurricane Danielle to the north, which caused Earl's outflow to be situated mainly to the south and west. The shear decreased throughout the day on 29 August as Danielle moved northward, allowing Earl to reach hurricane status. By 30 August warm SSTs and low shear caused Earl to rapidly intensify into a Category 4 hurricane. Earl weakened a bit on 31 August as it began an eyewall replacement cycle. The slight weakening was also enhanced by dry mid- and upper- level air approaching Earl from the north and increased southwesterly shear due to a weak trough over the eastern Bahamas. By 1 September the shear decreased as the trough in the Bahamas moved west. This decrease in shear combined with the warm ocean temperatures along Earl's track led to further intensification. An eye became very distinct and winds increased to 138 kt. By 5 a.m. on 2 September the MSLP was 928 hPa. During this time, Earl began to move northward into cooler waters. In addition, southwesterly shear of 15-20 kt was analyzed over the hurricane and dry air entrained through the southern semicircle from a deep trough approaching from the west. All of these factors weakened Earl and by 4 September, it turned extratropical (Cangialosi 2010).

Not only did Hurricane Earl experience warm ocean water, moist mid-level air and low shear when it rapidly intensified, but the genesis location of Earl was favorable for the maintenance and eventual intensification of the TC. Chen (2006) describes the concept of a northern and southern wave. A northern wave, which is an African Easterly Wave (AEW) that develops north of the African Easterly Jet (AEJ), generally experiences the negative effects of the dry air from the Saharan Air Layer (SAL). Therefore, development of these waves is suppressed, sometimes to the extent of dissipation. On the other hand, southern waves, which are AEWs that develop south of the AEJ, do not experience the negative effects of the SAL and therefore, have a greater chance of intensification. Hurricane Earl was a southern wave so it did not experience the negative effects of the SAL. Fig. 3a displays plotted streamlines at 600 hPa with the AEJ shown in orange at the genesis time. Fig. 3b corresponds to the accumulated 6-hour precipitation. Notice that precipitation was present at the genesis time and location, but a closed circulation was not defined at 850 hPa. Hurricane Earl developed as the AEW remained south of the AEJ throughout the forecast period (Fig. 3c). The precipitation continued for the next five days as the AEW traveled off the western coast of Africa. Note that by 24 August, the AEW was still south of the AEJ, the precipitation was more extensive, and a closed system developed (Figs. 3c and 3d). Because the AEW did not experience the harmful effects of the dry air from the SAL, the AEW could develop in the mid-troposphere. Eventually, the continued development led to the formation of Hurricane Earl. Overall the low shear, warm ocean water, moist mid-level air, and the fact that Earl was a southern wave all contributed to the potential for Hurricane Earl to rapidly develop.

5. Results

a. Observed thermodynamic profiles

Fig. 4 shows the vertical temperature profile for two representative dropwindsondes released in the outer rainband before RI. Both soundings are relatively moist near the surface and have vertical layers of comparatively dry air. The near surface layers are not saturated. and roughly constant wind speeds are present at every level, ranging from 15-35 kt. Fig. 4b is moister than Fig. 4a throughout the

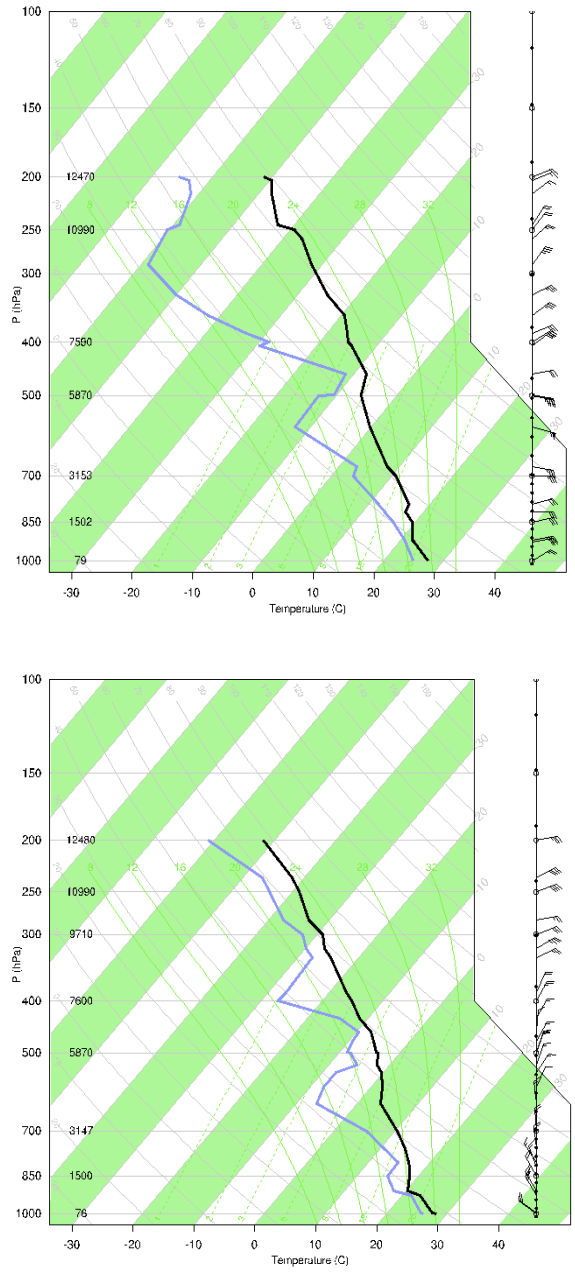

FIG. 4. Skew T–log p diagram of the outer rainband sounding of Hurricane Earl before RI at (top) 2214 UTC on 28 Aug. 2010 and (bottom) 2359 UTC on 28 Aug. 2010.

column, especially in the mid- to upper-troposphere, simply because this dropwindsonde was released above a region of convection within the outer rainband.

Fig. 5 corresponds to temperature soundings of dropwindsondes released in the eye (a), eyewall (b), and outer-rainband (c) during RI and post-RI (d)–(f). Note that the eye and eyewall soundings do not have data extending to the top of the troposphere, as the flight scientists released the dropwindsondes at lower levels for these locations. During RI, the eye already exhibits a subsidence-induced dry layer in the mid-troposphere. The development of this dry layer is evidence of an intensifying TC because adiabatic warming lowers the MSLP and intensifies the TC (Willoughby 1998). The temperature increases substantially from RI to post-RI, about 6 K, suggesting that a warm core is developing in the mid-troposphere. After RI, the mid-tropospheric dry layer is more pronounced with the creation of a subsidence-induced inversion. The near-surface layer has become saturated, most likely due to the exchange of moist enthalpy with the sea and air from the eyewall. Also evident are relatively weak winds throughout the vertical depth of the sounding, which is generally the case for winds in the eye.

The eyewall temperature soundings (Figs. 5b and 5e) do not change much from RI to post-RI. Both soundings are generally saturated throughout the vertical column, with the post-RI sounding having a moister near-surface layer. This sounding also has stronger near-surface winds, approaching 100 kt at 925 hPa, suggesting that Hurricane Earl is stronger during post-RI. This makes sense, as the MSLP continued to decrease after RI ceased (Fig. 1).

The dropwindsonde soundings in the outer-rainband (Figs. 5c and 5f) are comparable to those before RI in Fig. 4. All of these soundings have roughly the same temperature, lapse rate, and wind speed throughout the column. During RI, the vertical profiles are moister than the soundings before and after RI, especially in the mid- and upper-troposphere, suggesting that more enthalpy-rich air is advected to the center of Hurricane Earl during RI.

b. Comparison of observed and modeled temperature profiles

Observed and modeled temperatures were compared for all dropwindsondes at every mandatory level to investigate what caused the difference in the MSLP between the HWRF model and observations. Fig. 6a–d shows the MSLP and temperature differences for each dropwindsonde before RI, during RI, and after RI at 850 hPa, 700

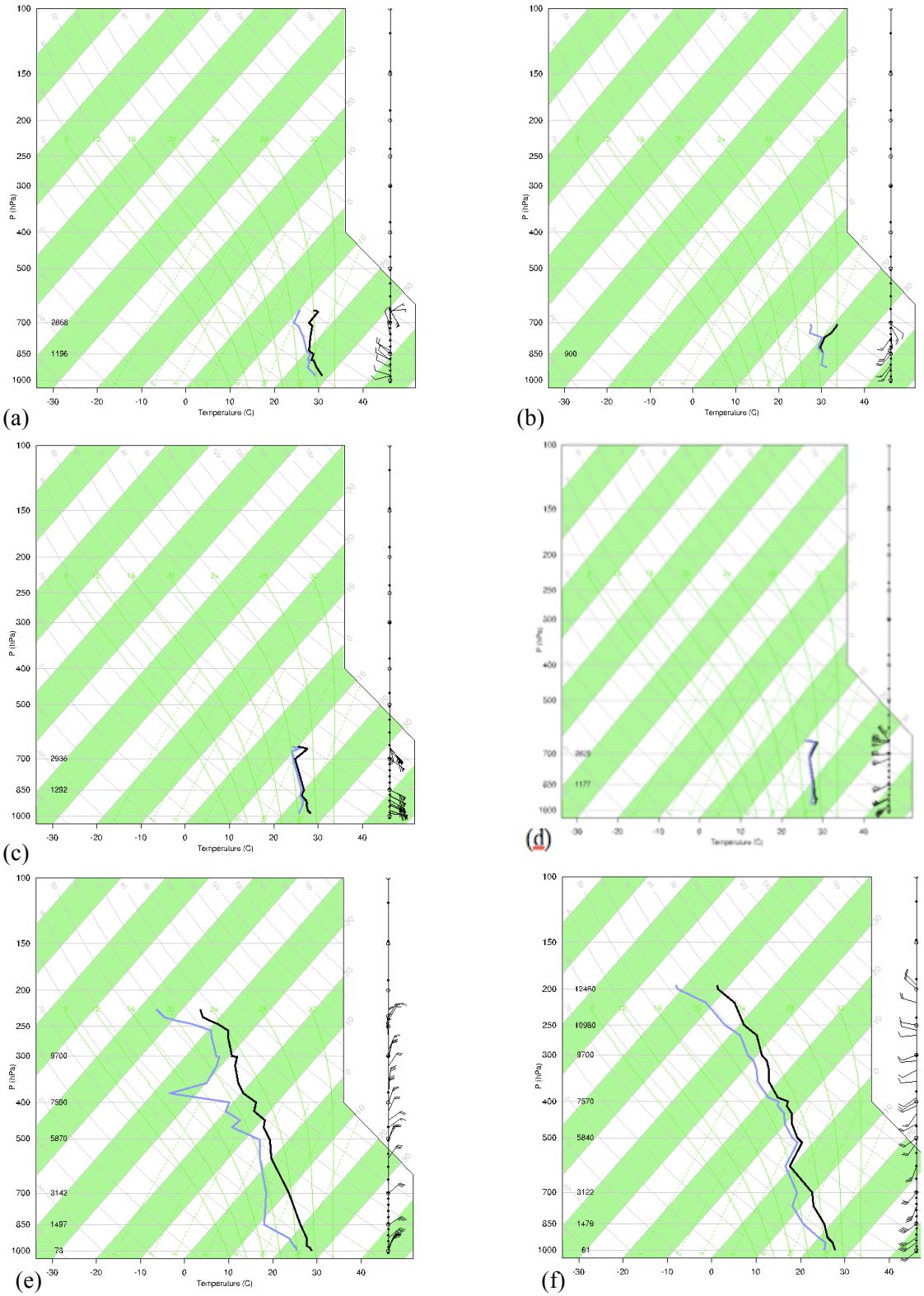

FIG. 5. Skew–T log p diagrams in the eye (a), eyewall (c), and outer rainband (e) during RI and in the eye (b), eyewall (d), and outer rainband (f) post-RI.

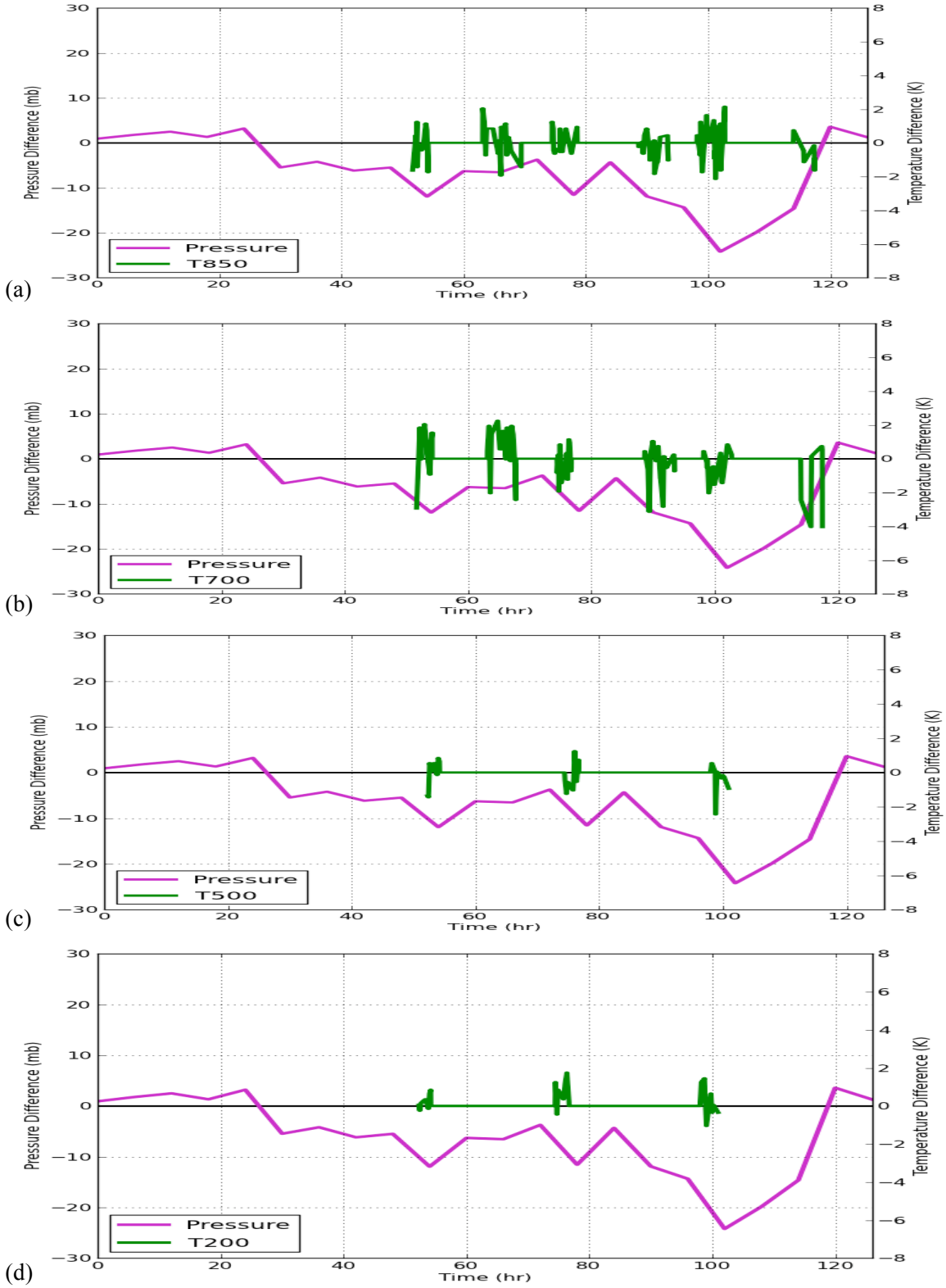

FIG. 6. Observed and modeled pressure (purple) and temperature (green) difference for the 126-hour forecast at (a) 850 hPa, (b) 700 hPa, (c) 500 hPa, and (d) 200 hPa.

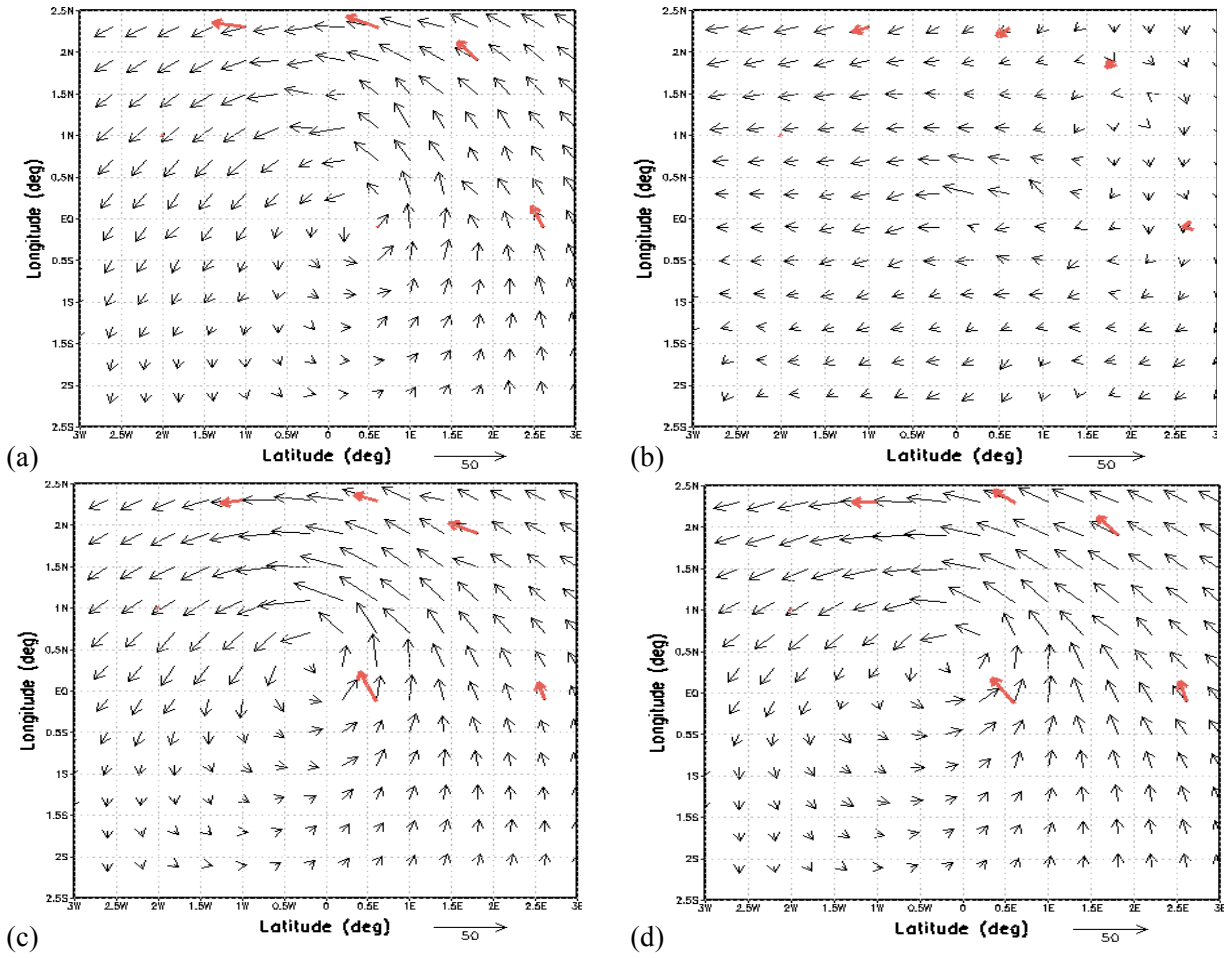

FIG. 7. Observed (black) and modeled (red) wind vectors at (a) 850 hPa, (b) 700 hPa, (c) 500 hPa, and (d) 200 hPa at 2240 UTC on 28 Aug. 2010.

hPa , 500 hPa, and 200 hPa, respectively. The large gaps corresponding to no temperature difference are when no dropwindsondes were released. Also note that there are fewer temperature differences at 500 hPa and 200 hPa. Flight scientists only released dropwindsondes at these higher levels in the outer rainband.

As is also shown in Fig. 1, the HWRF forecast accurately simulated the MSLP of Hurricane Earl during the first 25 hours of the forecast. Afterword, the magnitude of the pressure difference approached about 10 hPa for hours 25 through 85, with the modeled MSLP predicting higher values than the dropwindsonde observations. After hour 85 the HWRF model was more inaccurate, over-predicting the MSLP by about 24 hPa by hour 102. In theory, the temperature difference at each time should correlate with the difference in the MSLP. Most of the results at each mandatory level suggests otherwise. For example, the temperature differences at 850 hPa fluctuates around the zero line, suggesting that the difference in MSLP is not caused by the difference in the 850 hPa temperatures. Additionally, the temperature differences at 850 hPa have a mean of -0.07 K. This further suggests that the MSLP difference is not caused by the difference in the 850 hPa temperatures, since a negative temperature difference would imply that the modeled temperatures were warmer than observations. This would correspond to a positive MSLP difference, which is not the case for this forecast. The temperature differences at 700 hPa and 500 hPa are similar to the 850 hPa temperature differences. Again, the differences fluctuate around zero, with means of -0.19 K and -0.25 K for 700 hPa and 500 hPa, respectively. These negative averages do not

give insight into why the model consistently over-predicted the MSLP from hours 25 to 117.

The 200 hPa temperature differences are mostly positive with a few of the differences below the zero line. The average temperature difference is 0.4125 K, suggesting that the temperature difference at 200 hPa could correspond to the over-prediction of the MSLP by the HWRF model. However, note that the temperature differences do not increase in magnitude during the period of largest over-prediction (hour 102), implying that these temperature differences may not contribute to the differences in the observed and modeled MSLP. A two-sided t-test is completed to determine if there is a correlation between the temperature and MSLP differences, which gives a t-ratio of -0.09 of a p-value of 0.9255. Therefore, the 200 hPa temperature differences do not statistically correlate with the differences in the MSLP.

c. Comparison of observed and modeled wind speed and direction profiles

Wind speed and direction differences were examined at all of the mandatory levels to determine if these differences correlated with the MSLP differences.

Fig. 7 displays the observed and modeled wind vectors at every mandatory level. The center of Hurricane Earl corresponds to 0° latitude and longitude. Note that this is not the actual latitude and longitude of the TC but is the simulated latitude and longitude of the moving 3-km model nest, where the center of the TC is always at the center of the moving domain. Note that the modeled vectors are valid at 2240 UTC on 28 August. There are five dropwindsonde vectors plotted at 850 hPa and 700 hPa and four plotted at 500 hPa and 200 hPa. These dropwindsondes were released within 17 minutes of the plotted modeled vectors, so these vectors can be directly compared with the modeled data. Generally, the HWRF model successfully simulates the wind direction in the outer rainband at 850 hPa, 700 hPa, and 500 hPa. The wind speed is also well-simulated in the outer rainband, except for a negative bias at 500 hPa. The modeled wind speed and direction are inaccurate in the eyewall, as the model under-predicts the wind speed and the degree of inflow. These discrepancies may have altered the amount of enthalpy-rich air advected into the center of the TC, which could be the reason why there is a difference in the modeled and observed MSLP. At 200 hPa, the HWRF model accurately predicts the light wind speeds. Notice that the circulation of Hurricane Earl is not resolved at 200 hPa, probably because the circulation is not deep enough on 28 August (pre-RI) to penetrate this level.

In theory, a faster observational wind speed compared to the HWRF model would result in a lower MSLP. More enthalpy-rich air would be advected to the eyewall, which would increase convergence. In turn, this would increase the number of thunderstorms, increase the latent heat release, and increase the resultant warming in the eye, thus decreasing the MSLP compared to the model. This scenario would produce the negative pressure difference that is observed from hour 25 to 117.

Overall, every mandatory level suggests that the differences in wind speed between observations and the HWRF model could result in the MSLP differences, as the wind speed differences generally have a positive bias (Fig. 8). Note that the wind speed difference is large at times, with some differences as great as -40 kt and 40 kt, a range of 80 kt. The mean wind speed differences are 0.54 kt, 1.37 kt, 5.60 kt, and 2.93 kt for 850 hPa, 700 hPa, 500 hPa, and 200 hPa, respectively. These positive values indicate that the observed wind speed is greater than the modeled wind speed, on average. However, during the largest differences in MSLP (around hour 102), the differences in wind speed do not increase at any level. In some cases, the differences actually decrease (850 hPa and 200 hPa) and in other cases, the differences actually fall below zero (700 hPa). Negative wind speed differences does not make sense, as this would mean that the modeled wind speed would be greater than the observed wind speed. Theoretically, this would imply that the modeled MSLP would be less than that observed (positive difference), as a faster modeled wind speed would warm the core of the TC faster.

Statistical testing is conducted to determine if there is a statistically significant linear relationship between the observed and modeled wind speed differences and MSLP differences. Resulting t-ratios and p-values are shown in Table 1, which suggests that none of the levels have a statistically significant result.

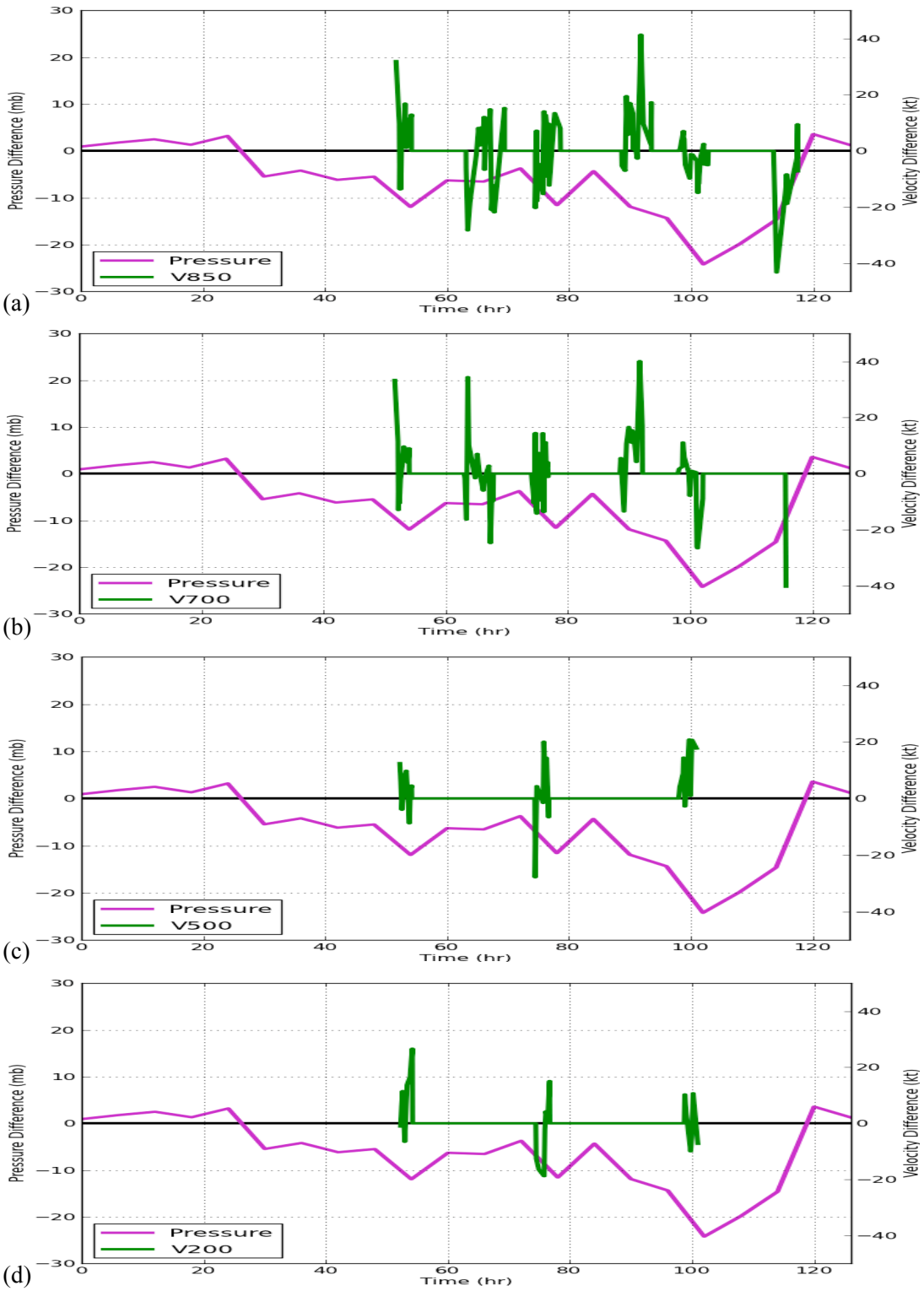

FIG. 7. Observed and modeled pressure (purple) and wind velocity (green) difference for the 126-hour forecast at (a) 850 hPa, (b) 700 hPa, (c) 500 hPa, and(d) 200 hPa.

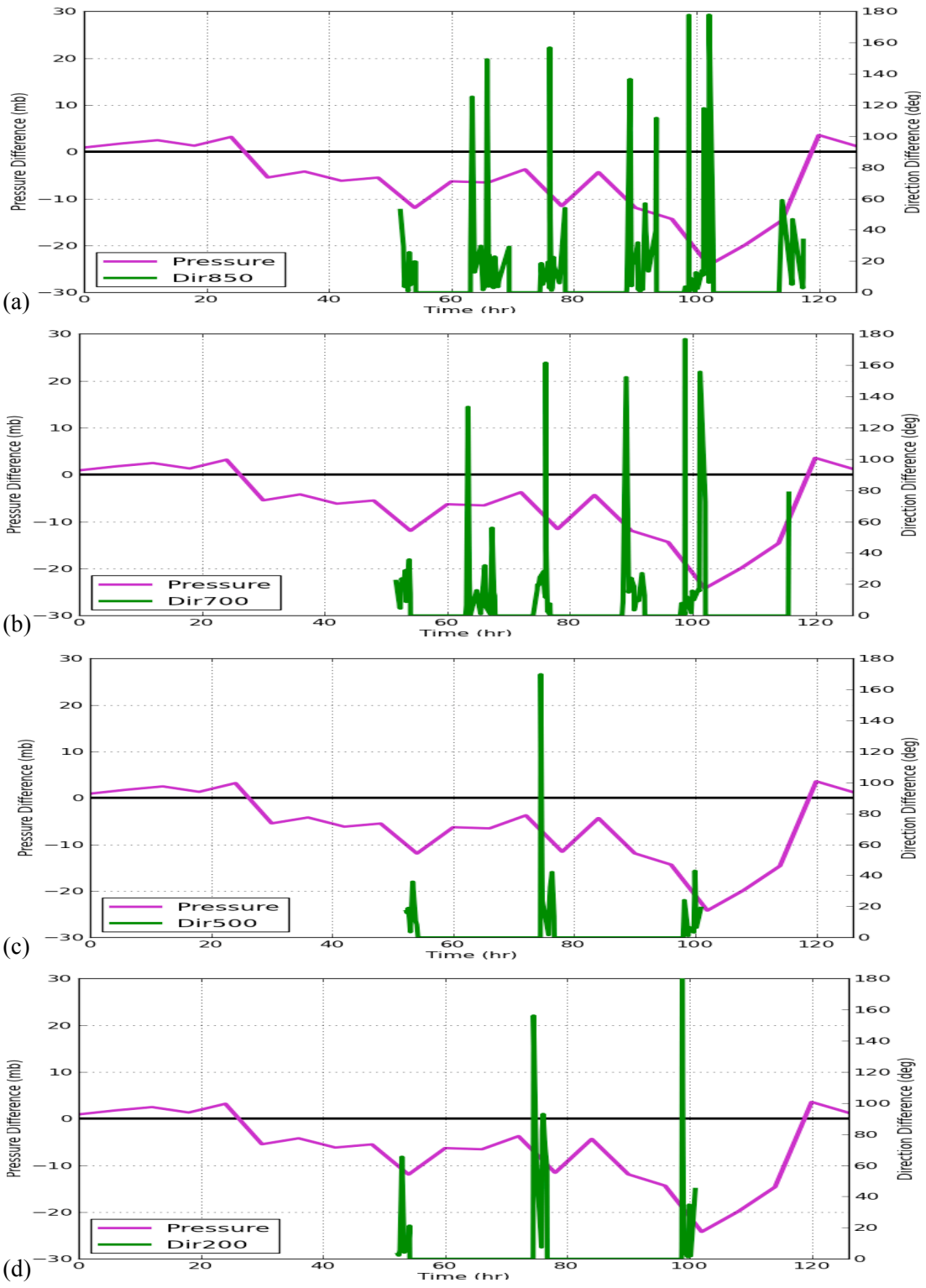

FIG. 8. Observed and modeled pressure (purple) and wind direction (green) difference for the 126-hour forecast at (a) 850 hPa, (b) 700 hPa, (c) 500 hPa, and(d) 200 hPa.

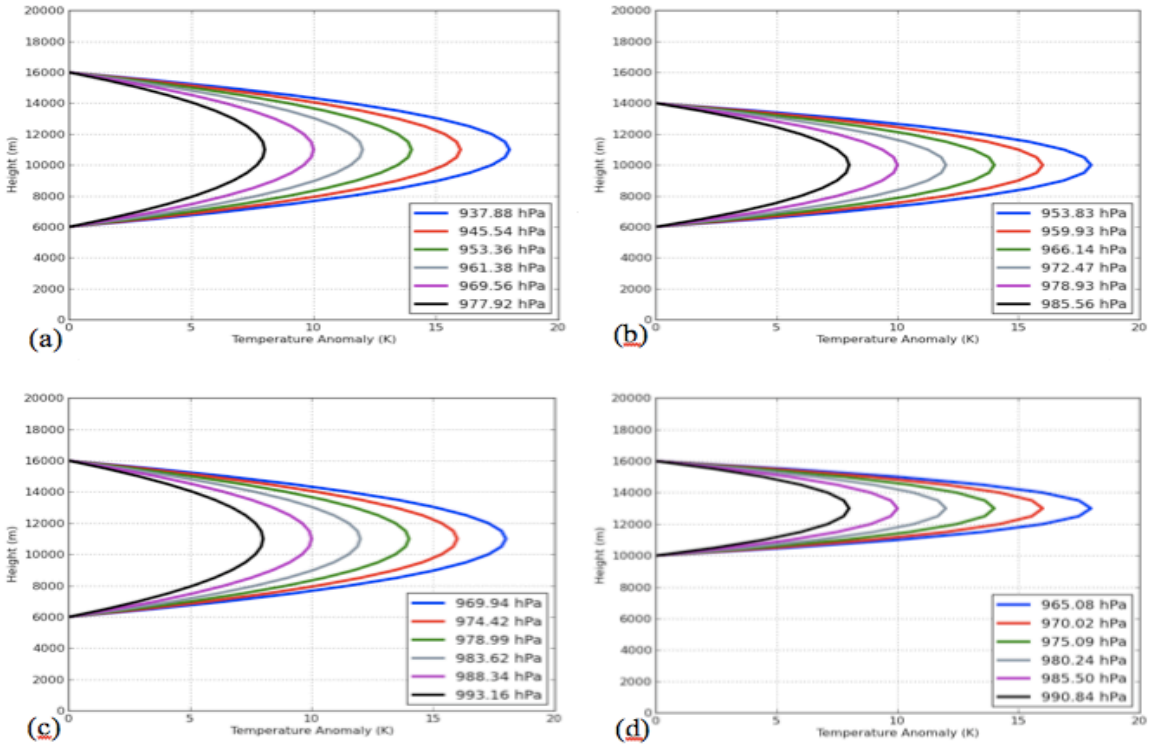

FIG. 9. (a) Idealized parabolic warm cores with a vertical depth from 6000 m to 16000 m, (b) vertical depth from 6000 m to 14000 m, (c) vertical depth from 6000 m to 12000 m, and (d) vertical depth from 1000 m to 16000 m. Each colored parabola represents a different maximum temperature anomaly, with blue, orange, green, grey, purple and black corresponding to 18 K, 16 K, 14 K, 12 K, 10 K, and 8 K, respectively. The resulting MSLP for each parabola is shown.

Variable	T-ratio	P-value
V850	1.11	0.27
V700	1.06	0.30
V200	0.50	0.63
Dir850	1.30	0.20
Dir700	0.59	0.56
Dir500	0.13	0.90
Dir200	0.29	0.78

TABLE 1. t-ratios and corresponding p-values for 2-tailed t-tests.

As shown in Fig. 7, the HWRF model did not accurately simulate the wind direction of the observational data in the eyewall. Therefore, the MSLP differences may be due to differences in the wind direction between observations and the model. In theory, the MSLP differences should increase in magnitude as the differences in wind direction increase since a different wind direction in the model would advect enthalpy-rich air to a separate part of the storm. For example, in Fig. 7 it is probable that the model advected less moisture into the eye of Hurricane Earl due to less inflow. This would result in less convergence near the eye, resulting in less thunderstorms and latent heat release to lower the MSLP.

Fig. 9 shows the wind direction differences overlaid on the MSLP differences. In general, the differences in wind direction oscillate between 0° and 50° with time. At 850 hPa, the differences in wind direction increase at the onset of the large drop in the MSLP differences, suggesting that a different wind direction at 850 hPa produces this pressure difference. This is also the case for 700 hPa and 200 hPa, although it is better depicted at

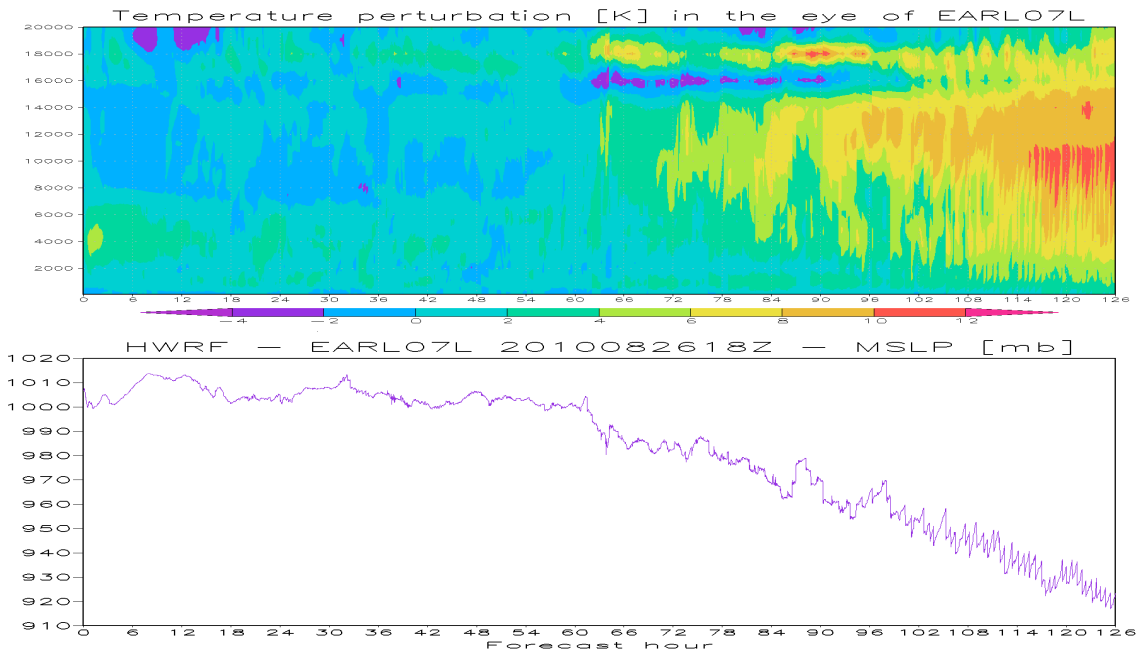

FIG. 10. (top) Hurricane Earl's warm core structure for the 126-hour forecast starting at 18 UTC on 26 August and (bottom) the resulting MSLP for the same forecast period.

850 hPa. At the 500 hPa level, the differences in wind direction stays relatively constant with time, suggesting that this level does not offer insight into the mechanism behind the drop in the MSLP differences. The resulting statistical tests at 850 hPa, 700 hPa, and 200 hPa are displayed in Table 1. Again, there is no significant linear correlation between the differences in wind direction and differences in MSLP for any of these levels.

d. Warm core structures

1) IDEALIZED WARM CORE

Fig. 10 shows idealized parabolic warm core structures in a vertical depth of the atmosphere relative to the standard atmosphere temperature profile. There are six parabolas per graph, each corresponding to a slightly different warm core structure. For example, the blue parabola has a maximum temperature anomaly of 18 K while the black parabola has a maximum temperature anomaly of only 8 K.

The corresponding MSLPs are recorded in Fig. 10a–d. There are two interesting findings. First, the development of an upper-level warm core does not significantly lower the MSLP (Figs. 10c and 10d). These figures both have warm core depths of 6000 m, but the warm cores in Fig. 10d are positioned 4000 m higher than those in Fig. 10c. The corresponding MSLPs in Fig. 10d are only slightly less than those in Fig. 10c. For example, the MSLP for the 18 K maximum temperature anomaly curves only differ by 4.86 hPa. Similar results occur for the other warm core structures in Figs. 10c and 10d. Although these results suggest that an upper-level warm core is slightly more effective than a lower-level warm core in reducing the MSLP, the MSLP is not as sensitive to the height of the warm core as discussed in Zhang and Chen (2012). Figs. 10a–c have warm core structures that begin at 6000 m, but vary in depth. Fig. 2c has a warm core depth of only 6000 m, while Figs. 10b and 10a have depths of 8000 m and 10000 m, respectively. In comparing these figures, it seems that the main factor in lowering the MSLP is the depth of the warm core. The MSLPs in Fig. 10a are significantly lower than those corresponding to shallower warm cores. For the 18 K maximum temperature anomaly cases, the MSLP in Fig. 10a is 15.95 hPa lower than in Fig. 10b and 32.06 hPa lower than in Fig. 10c. This finding suggests that the combined effects of a deep warm core are more effective in lowering the MSLP than having a warm core at a high level. Note that this effect is less significant for a weaker warm core, say for a maximum temperature anomaly of 8 K. For this

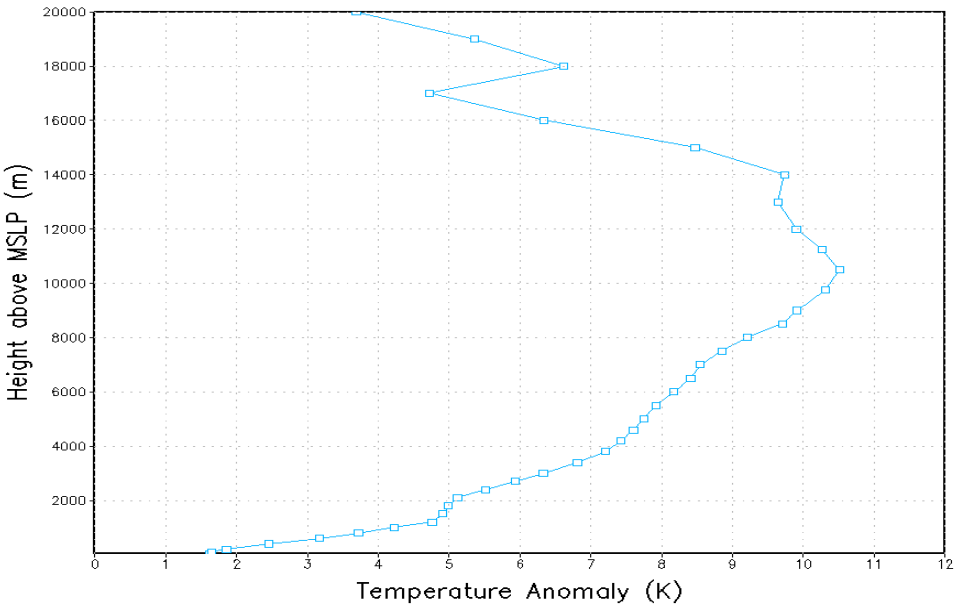

case, the resulting MSLP is only 7.64 hPa lower in Fig. 10a than in Fig. 10b and only 15.24 hPa lower than in Fig. 2c. Nonetheless, this warm core is still more effective in lowering the MSLP than a higher-level warm core.

2) HURRICANE EARL'S MODELED WARM CORE

Fig. 11 shows Hurricane Earl's modeled warm core structure from forecast hour 0 to 126 with the corresponding drop in MSLP (Fig. 11). This figure represents the temperature anomaly at the center of the high-resolution nest every minute, which is assumed to be the center of Earl's warm core. Clearly, the MSLP decreases as the warm core develops. It is evident how the warm core develops from Fig. 11. At about hour 63, the warm core begins to quickly strengthen from roughly 8000 to 14000 m. This development corresponds to a drop in MSLP from 1003.81 hPa to 980.42 hPa in just over 2 hours and represents the onset of RI in the model. The warm core expands vertically outward as time progresses and by the last forecast hour, it extends through the depth of the troposphere. Interestingly, the maximum temperature anomaly at hour 126 is in roughly the same location as the developing warm core at hour 63, suggesting that the maximum temperature anomaly was stagnant through the RI period. After hour 70 the warm core gradually develops and by hour 126, reaches a value of 10.51 K at 10500 m. The frequent oscillation of MSLP in Fig. 11b suggests that small-scale fluctuations were occurring in the warm core possibly from isolated warm (cold) pockets of air that decreased (increased) the MSLP, or may have been the result of diurnal fluctuations. Nonetheless, note that the warm core gradually strengthens, which produces a steady decrease in the MSLP.

Fig. 12 shows Earl's warm core at the final forecast hour. The temperature anomaly extends from the surface to 20000 m, as it does in Fig. 11a. Of importance is the depth of the warm core. A temperature anomaly of 5 K or greater extends from roughly 2100 m to 16750 m, and a positive anomaly extends through the depth of the column.

6. Conclusions

This study aimed to understand the observed and modeled rapid intensification of Hurricane Earl, particularly during RI. Vertical temperature profiles for every dropwindsonde released before, during, and after RI showed the development of a subsidence-induced dry layer in the eye and saturation within the eyewall. Due to the unprecedented dropwindsonde dataset, this is the first study known to examine the evolution of a TC before, during, and after RI. Forecasters at the NHC can use these results when studying in-time dropwindsonde data to determine if a TC will likely intensify.

This study also compared observational and modeled vertical thermodynamic and dynamic profiles to analyze what caused the difference in the modeled MSLP compared to the observtions. Results suggest that neither the discrepancy in the modeled temperature, wind speed, or wind direction at any of the mandatory levels provides statistically significant information on this question, refuting the stated hypotheses. Therefore, the HWRF model may have simulated a different variable incorrectly, which is corresponding to the differences in the observed and modeled MSLP. Maybe the differences are the result of multiple factors, such as the combined temperature differences throughout the vertical column. Conversely, the differences may be due to the lack of physical parameterizations to represent the true atmosphere or some other factor. It is clear that modeling TC intensification is a tough objective, especially because it is so difficult to understand why the modeled forecast varied from reality.

Lastly, this study analyzed idealized parabolic warm cores to suggest how the development of a warm core influences the MSLP. Based on the results, the depth of the warm core is the most important factor in lowering the MSLP, not the height. Hurricane Earl rapidly intensified due to the expanding depth of its warm core. Forecasters at NHC can use these findings to more accurately predict the intensity of a TC, given the magnitude and depth of its warm core.

7. Next Steps

Other variables should be studied to determine what caused the modeled MSLP to differ from observations. One could manipulate parameterization schemes to produce a more accurate modeled forecast. Additionally, a comparison of the temperature, wind speed, and wind direction differences should be analyzed through the entire vertical column. Taking differences only at mandatory levels may not be representative of the true differences.

Furthermore, it is important to repeat this study using different TCs. An analysis of one TC cannot determine the inaccuracies of a model, as any model performs well and poor in different situations. Thus, more TCs should be studied to conclude what is causing the HWRF forecast to differ from observations.

Acknowledgements. Thank you to my mentors at HRD, Drs. S. Gopalakrishnan, T. Quirino, H. Chen, and X. Zhang, for motivating me to pursue this research topic, providing useful HWRF model data, and guiding me through this study. Thank you to Drs. T.-C. Chen and P. Tsay for their support, suggestions, and computer programming help. Additionally, thank you to HRD's K. Sellwood for providing the dropwindsonde data.

REFERENCES

Chen, T.-C., 2006: Characteristics of African Easterly Waves Depicted by ECMWF Reanalyses for 1991–2000. *Mon. Wea. Rev.*, **134,** 3539–3566.

Haurwitz, B., 1935: The height of tropical cyclones and of the "eye" of the storm. *Mon. Wea. Rev.*, **63,** 45-49.

Holliday, C. R., and A. H. Thompson, 1979: Climatological characteristics of rapidly intensifying typhoons. Mon. *Wea. Rev.*, **107,** 1022–1034.

Holton, J. R., 2004: *An Introduction to Dynamic Meteorology*. Elsevier Academic Press, 535 pp.

Houze, R. A., S. S. Chen, W.-C. Lee, R. F. Rogers, J. A. Moore, G. J. Stossmeister, M. M. Bell, J. Cetrone, W. Zhao, and S. R. Brodzik, 2006: The Hurricane Rainband and Intensity Change Experiment: Observations and modeling of Hurricanes Katrina, Ophelia, and Rita. *Bull. Amer. Meteor. Soc.*, **87,** 1503–1521.

Gopalakrishnan, S. G., F. Marks Jr., X. Zhang, J.-W. Bao, K.-S. Yeh, and R. Atlas, 2010: The experimental HWRF System: A study on the influence of horizontal resolution on the structure and intensity changes in tropical cyclones using an idealized framework. *Mon. Wea. Rev.*, **139,** 1762–1784.

Gopalakrishnan, S. G., N. Surgi, R. Tuleya, and Z. Janjic, 2006: NCEP's two-way-interactive-moving-nest NMM-WRF modeling system for hurricane forecasting. Preprints, *27th Conference on Hurricanes and Tropical Meteorology*, Monterey, CA, Amer. Meteor. Soc., Ar. 7A.3.

Gopalakrishnan, S. G., X. Zhang, K.-S. Yeh, T. S. Quirino, F. D. Marks Jr., S. B. Goldenberg, and S. Aberson, 2011: HWRFX: Improving hurricane forecasts with high-resolution modeling. *Computing in Science & Engineering*, **13**, 13-21. R.K. Smith, 1980: Tropical Cyclone Eye Dynamics. *J. Atmos. Sci.*, **37,** 1227–1232.

J. P. Cangialosi, 2010: Tropical cyclone report Hurricane Earl. National Hurricane Center, 26 pp.

Kaplan, J., and M. DeMaria, 2003: Large-scale characteristics of rapidly intensifying tropical cyclones in the North Atlantic basin, *Wea. Forecasting*, **18,** 1093–1108, doi: http://dx.doi.org/10.1175/1520-0434(2003)018<1093:LCORIT>2.0.CO;2.

Krishnamurti, T. N., A. Simon, M. K. Biswas, and C. Davis, 2012: Impacts of cloud flare-ups on hurricane intensity resulting from departures from balance laws. *Tellus A*, **64,** 18399, http://dx.doi.org/10.3402/tellusa.v64i0.18399.

Montgomery, M.T., V. S. Nguyen, J. Persing, and R. K. Smith, 2009: Do tropical cyclones intensify by WISHE? *Quart. J. Roy. Meteor. Soc.*, **135**, 1697–1714.

Nguyen, V. S., R. K. Smith, and M. T. Montgomery, 2008: Tropical-cyclone intensification and predictability in three dimensions. *Quart. J. Roy. Meteor. Soc.*, **134,** 563–582.

Smith, R. K., M. T. Montgomery, and S. Vogl, 2008: A critique of Emanuel's hurricane model and potential intensity theory. *Quart. J. Roy. Meteor. Soc.*, **134,** 551-561.

Smith, R. K., M. T. Montgomery, and N. V. Sang, 2009: Tropical cyclone spin-up revisited. *Quart. J. Roy. Meteor. Soc.*, **135**, 1321–1335.

Willoughby, H. E., 1998: Tropical cyclone eye thermodynamics. *Mon. Wea. Rev.*, **126,** 3053–3067.

Zhang, D.-L. and H. Chen, 2012: Importance of the upper-level warm core in the rapid intensification of a tropical cyclone. *Geophys. Res. Lett.*, **39,** L02806, doi:10.1029/2011GL050578.